Original Article

Pablo R. Seré, Paola Pary, Erasmo Gámez-Espinosa, Walter Egli, Alejandro R. Di Sarli and Cecilia Deyá*

Surface preparation and double layer effect for silane application on electrogalvanized steel

https://doi.org/10.1515/corrrev-2022-0042
Received June 10, 2022; accepted March 31, 2023;
published online May 9, 2023

Abstract: Silanes are an alternative to replace pretreatments based on Cr(VI) for electrogalvanized steel (ES). As the interaction between the silane and the metal is important to ensure pretreatment efficiency, surface preparation is a critical step. In this sense, the presence of OH groups on the metal surface is essential. In this paper, the surface preparation of ES and a single/double layer application on the corrosion protection afforded by 3-aminopropyltriethoxy silane was studied. The metal surface was cleaned by polishing, electrochemically (employing anodic or cathodic current) or by chemical oxidation. The electrochemical behavior of the cleaned surfaces was analyzed by cyclic voltammetry and electrochemical impedance spectroscopy (EIS). Afterwards, the hydrolyzed silane was applied in a single or double layer. Coatings were characterized by scanning electron microscopy and energy dispersive X-ray spectroscopy, EIS and by exposure to the humidity chamber. Coatings applied on ES cleaned by electrochemical anodic processes or chemical oxidation provided the best protective performance due to a lower surface of zinc exposed to the high humidity environment. Double layer coatings improved protection due to more homogeneous and higher Si content, sealing defects and increasing the thickness of the one-layer protection, enhancing the barrier protection of the silane.

Keywords: double layer coatings; electrochemical cleaning; electrogalvanized steel; oxidizing cleaning; silane pretreatment; surface cleaning.

***Corresponding author: Cecilia Deyá**, Centro de Investigación y Desarrollo en Tecnología de Pinturas (CIDEPINT), CICPBA-CONICET La Plata-UNLP, Av. 52 s/n entre 121 y 122, B1900AYB La Plata, Argentina; and Facultad de Ingeniería, Universidad Nacional de La Plata, Av. 1 esq. 47, B1900TAG La Plata, Argentina, E-mail: c.deya@cidepint.ing.unlp.edu.ar. https://orcid.org/0000-0003-2853-5982

Pablo R. Seré, Erasmo Gámez-Espinosa, Walter Egli and Alejandro R. Di Sarli, Centro de Investigación y Desarrollo en Tecnología de Pinturas (CIDEPINT), CICPBA-CONICET La Plata-UNLP, Av. 52 s/n entre 121 y 122, B1900AYB La Plata, Argentina. https://orcid.org/0000-0003-4092-4198 (E. Gámez-Espinosa)

Paola Pary, Centro de Investigación y Desarrollo en Tecnología de Pinturas (CIDEPINT), CICPBA-CONICET La Plata-UNLP, Av. 52 s/n entre 121 y 122, B1900AYB La Plata, Argentina; and Facultad de Ingeniería, Universidad Nacional de La Plata, Av. 1 esq. 47, B1900TAG La Plata, Argentina

1 Introduction

One way to protect steel from corrosion is by the application of a thin zinc layer that acts as a physical barrier and confers sacrificial protection to steel. This steel-zinc combination is known as galvanized steel. However, zinc corrodes forming non-protective compounds (white rust) in the presence of humidity. So, in order to enhance steel´s protection afforded by the zinc layer, another protective treatment must be done on galvanized steel (Saravanan and Srikanth 2019).

Chromate coatings have been used on several metals to protect them from corrosion. The formation of the chromate coating on zinc substrates involves the oxidation and dissolution of the zinc surface in the chromating solution and the evolution of hydrogen, that reduces a certain amount of Cr(VI) to Cr(III). The protective film formed is considered as a complex mixture consisting of hydrated basic chromium chromate, hydrous oxides of Cr(VI) and Cr(III) and the basis metal (Saravanan and Srikanth 2019; Zeller and Savinell 1986). The protection afforded by this film is due both to the corrosion inhibiting effect of Cr(VI) contained in the film and to the physical barrier presented by the film itself. Even scratched or abraded films retain a great deal of their protective value due to the presence of the hexavalent chromium [post treatment]. However, although Cr(VI) coating is highly effective, it is very toxic and carcinogenic (Public Health Service 2010).

The application of functionalized silane-, Cr(III)-, Ce(III)-, La(III)- based solutions, silica nanoparticles or nanocontainers (Akhtar et al. 2018; Figueira 2020; Hesamedini and Bund 2019; Niknahad and Mannari 2016; Thai et al. 2020; Yu et al. 2020; Zandi Zand et al. 2016) seem to constitute one of the best alternatives to replace Cr(VI)-based pretreatments

and to provide temporary protection against corrosion of metals such as zinc, steel, magnesium, aluminum and its alloys (Alibakhshi et al. 2018; Gao et al. 2019; Jeyaram et al. 2020; Ramezanzadeh et al. 2017; Younis et al. 2013; Zhao et al. 2021b).

Conversely, although the silanes provide protection only by acting as a physical barrier (Dave et al. 2004; Gao et al. 2019; Seré et al. 2016; Seré et al. 2014b), they are not toxic, nor contaminant, have a good thermal stability and hardness (Gao et al. 2019). The barrier properties of the silane film are due to the compact film formed on the metallic substrates and its tenacious adhesion that delays the ingress of corrosive compounds such as moisture, oxygen, chlorides, etc. (Nejad et al. 2022; Saravanan and Srikanth 2019; Vuori et al. 2016). In these applications, one of the most common reaction stages is the silane molecule hydrolysis which leads to the formation of highly reactive silanol groups. These groups react with the metal substrate oxides and hydroxides forming Silica-Oxygen-Metal (Si–O–M) bonds (van Ooij et al. 2005; Wang and Bierwagen 2009). Crosslinking also occurred among the silanols, forming Si-O-Si covalent bonds (Owczarek 2019; Pathaka et al. 2006; Yu et al. 2020).

In practice, the most common organo-functional groups present in a silane molecule are: –SH, –OH, $–NH_2$ $–CHOCH_2$, –COOH. Typically, a requirement is that the silane's organo-functional group does not interact with the substrate surface to be available towards the outer surface, providing the film formed interaction with the painting system, adhesion, hydrophobicity, etc.

The protection afforded by the silanes can be improved by the incorporation of organic (mercaptobenzothiazole, thiosalicylic acid), inorganic (zinc and rare earth ions), "green" inhibitors (plant extracts) and nanoparticles to the silane film (Asadi and Naderi 2020; Calabrese and Proverbio 2019; Khramov et al. 2005; Nikpour et al. 2018; Owczarek 2019; Pathaka et al. 2006; Peng and Man 2009). Besides, bis-silanes and mixtures of silanes were also studied alone or doped with inhibitors (Wang et al. 2012; Yu et al. 2020). The enhance in the protection afforded by the doped silane film maybe due to a reduced porosity, an increased coating thickness, and/or formed extra protective film due to the reaction of the substrate with the leached inhibitor (Asadi and Naderi 2020; Nikpour et al. 2018; Owczarek 2019).

As silanes protect mainly due to a physical barrier, the anticorrosive protection capacity given to the substrate depends on the film porosity and thickness and on the silane nature. The presence of hydrophobic or hydrophilic chains in the silane chemical structure can control the water diffusion rate through the coating film. Moreover, when the silane molecule is adequately selected, adhesion between metal and the painting system can be significantly improved (Gladkikh et al. 2020; Sundararajan and van Ooij 2000; van Ooij et al. 2000; Wang et al. 2019). Furthermore, substrate characteristics, such as metal roughness, structure and surface composition, should be considered since the silane adhesion to the metal could be enhanced or reduced (Jussila et al. 2010; Tiringer et al. 2021).

Due to this fact, it is convenient to prepare the substrate to obtain a surface with a high density of hydroxyl groups. Many different cleaning methods, including alkaline solutions (some of them commercially available), polishing, and surface oxidation by heating, have been reported in the literature (Wang et al. 2012; Najari et al. 2012; Sundararajan and van Ooij 2000; van Dam et al. 2020; Wang et al. 2019). Some authors have conducted experiments on steel and aluminum using cleaning solutions with different alkalinity and showed that the amount of hydroxyl groups on the metal surface strongly affects the starting and growing of the silane films (van Ooij et al. 2005; Zhao et al. 2021a).

The aim of the present work is to study the efficiency of different cleaning methods used before the silane application. To this end, electrogalvanized steel sheets, of commercial quality, were used as substrate. The specimens surface was cleaned by: (a) polishing; (b) electrochemical cathodic process; (c) electrochemical anodic process; or (d) oxidizing process, developed by the Radio Corporation of America (Kern 1990; Najari et al. 2012). All the specimens were characterized by scanning electron microscopy (SEM) and energy dispersive X-ray spectroscopy (EDS), cyclic voltammetry (CV) and electrochemical impedance spectroscopy (EIS). Then, the silane film was applied by immersion once or twice for obtaining one or two layers, and the relative area of the exposed substrate was determined by cyclic voltammetry (CV). The corrosion protection level provided to the coated electrogalvanized steel was studied by EIS and specimen exposure to the humidity chamber (HC). No previous studies have investigated the influence of the zinc cleaning methods on the silane film performance.

2 Materials and methods

2.1 Preparation and characterization of the cleaned surfaces

Commercial electrogalvanized steel sheets (75 × 100 × 0.6 mm) were used as metallic substrate. The zinc thickness was 7 µm measured by gravimetry. The substrate was cleaned as follow:

(a) polished with G600 waterproof sandpaper for 1 min in distilled water at pH 7; polishing cleaning (P specimens).
(b) immersed in 10 % NaOH for 20 s at 40 °C with a cathodic current of 0.12 A/cm^2; a stainless-steel rod was used as anode; electrochemical cathodic process (C specimens).

(c) immersed in 10 % NaOH for 20 s at 40 °C with an anodic current of 0.12 A/cm^2; stainless-steel rod was used as cathode; electrochemical anodic process (A specimens).
(d) immersed in 0.01 mol/L HCl solution for 1 min at room temperature (22 ± 2 °C) and afterwards, in a RCA® ($NH_3/H_2O_2/H_2O$, 1/1/400) (Kern 1990, Najari et al. 2012) for 10 min at 80 °C; oxidizing process (RCA specimens).

After cleaning, the specimens were rinsed with distilled water, ethyl alcohol and finally dried by air jet.

These cleaning procedures were selected in order to produce different amounts of OH groups on the surface as it is claimed that the presence of OH on the metal surface enhance the silane adhesion (Jussila et al. 2010; Krzak et al. 2020; Tiringer et al. 2021). It is expected that the polishing method to clean the surface would not increase the amount of OH on surface.

The use of cathodic current would reduce all the oxides/hydroxides forming a natural layer on zinc, diminishing the amount of OH and acidizing the solution:

$$\text{Reduction of Zn (II)compounds} : Zn^{2+} + 2e^- \rightarrow Zn$$
$$\text{Oxidation of water} : H_2O \rightarrow O_2 + 2H^+ + 2e^-$$

The used of anodic current and oxidation conditions would partially oxidize the zinc, increasing the amount of oxide-containing species on the metal surface (Zhang 1996). The chemical reactions would be as follows:

$$\text{Oxidation of Zn} : Zn \rightarrow Zn^{2+} + 2e^-$$
$$\text{Reaction of water during anodic process} : 2e^- + 2H_2O \rightarrow H_2 + 2OH^-$$

During the oxidation process in RCA®, the reactions that would occur are the oxidation of Zn and the reduction of H_2O_2, in the presence of NH_3:

$$2e^- + H_2O_2 \rightarrow 2OH^-$$

In order to characterize the cleaned surfaces, specimens were observed by SEM using a Quanta 200® FEI microscope with an Apollo 40 electron detector, employing high vacuum conditions. The surface composition was determined by EDS using an EDAX® detector. Besides, the electrochemical behavior of the surfaces was evaluated by cyclic voltammetry in an aerated borate solution (35 g/L de H_3BO_3 and 40 g/L of $Na_2B_4O_7.10H_2O$) (Seré et al. 2014a; Titz et al. 2010). A cathodic swept was performed at 0.01 V/s from the open circuit potential (E_{op}) to −1.50 V versus Saturated Calomel Electrode (SCE). The peak observed at certain cathodic potential value is attributed to the reduction of zinc oxides/hydroxides generated during the surface cleaning process (Jiang et al. 2012; Zhang 1996).

EIS was also done on the cleaned specimens delimiting the metal surface in contact with the electrolyte to 15.9 cm^2. A Pt-mesh was used as counter-electrode and a SCE as reference. Tested specimens were exposed to a 0.05 mol/L NaCl solution at 22 ± 2 °C and the EIS measurements started after 20 min of immersion. Impedance spectra were obtained in the potentiostatic mode at the E_{op} using a sinusoidal signal with 10 mV peak to peak amplitude over the frequency range from 1.10^{-2} to 1.10^5 Hz. A Solartron 1255 FRA® coupled to a Potentiostat-Galvanostat Solartron 1286 EI®, both controlled by the Zplot® software, was used. Results adjustment to obtain equivalent circuits to model the physicochemical behavior of each system was made with the Z-View® program.

The first condition to reach an adequate adhesion between the silane and the metal surface is that when they will come into contact a molecular interaction takes place, reason for which the silane must properly wet the metal surface. This condition is obtained when $\gamma_L < \gamma_s$, being γ_L the liquid surface tension and γ_S the solid surface energy (Prane 1986). The wetting tension of cleaned specimens was estimated by applying on the solid surface a series of ethanol and water solutions drops and the surface tension of these solutions was quantified by the ring method (Du Noüy). This test consists of suspending horizontally a Pt ring in the flat surface of the evaluated liquid and measured the force necessary to separate the ring from the liquid surface (Freund and Freund 1930).

When a drop of liquid rests on a solid surface, and both are in contact with a gas, the forces acting at the interfaces must balance. These forces can be represented by surface energies acting in the direction of the interface and they follow Young's equation:

$$\gamma_{LV} \times \cos\ \theta = \gamma_{SV} - \gamma_{SL} \quad (1)$$

The contact angle θ of a distilled water drop applied on the cleaned surfaces was measured from photographs taken with a Gaosuo microscope, employing the Gaosuo´s software. The contact angle values can be associated to the surface hydrophilicity/hydrophobicity and it is related to the chemical groups present on it (Einati et al. 2009; Vuori et al. 2016).

2.2 Preparation and characterization of the silane films

Silane solution was prepared by adding 4 % v/v of 3-aminopropyltriethoxy silane (APTES, provided by CAMSI-X) to a solution containing distilled water/isopropanol (0.5/99.5 % v/v) at pH 10 (Chico et al. 2012; Vuori et al. 2016). The silane was hydrolyzed for 1 h under stirring. The surface tension of the hydrolyzed APTES was quantified by the ring method.

Cleaned specimens were immersed in the hydrolyzed silane solution for 1 min, dried under hot air and cured in oven at 80 °C for 10 min. The silane was not applied on some polished panels, which were employed as reference (P).

Considering the results obtained with the one-layer systems, some specimens cleaned with RCA® were immersed in the silane solution, left to dry, and immersed again for another minute. Then, these specimens were dried under hot air and cured in oven at 80 °C for 10 min.

The surfaces with silane were observed by the same electron microscope and the coated surface composition determined as before. The substrate active area was evaluated by cyclic voltammetry through a swept potential from –1.50 V to –0.50 V versus SCE carried out at 0.1 V/s, at room temperature. The solution was the same used to evaluate the electrochemical behavior of the cleaned specimens. In this aerated borate solution, the CV on zinc electrodes shows an anodic dissolution peak (Ap) followed by a passive region. The integration of this peak gives an anodic charge density proportional to the active zinc area (Seré et al. 2016).

The temporary protection degree provided by the silane film on the substrate of specimens cleaned with the RCA® process, and then coated with one or two layers of APTES, were tested through EIS. The set up was the same as for specimens without silane, but measurements were made after 20 min, and 4, 24 and 48 h of immersion. The impedance modulus value at low frequencies was selected as the assessment parameter of the system behavior against corrosion, because it is considered as the total system resistance (Barceló et al. 1998; Magalhães et al. 1999). Furthermore, accelerated test in the humidity and temperature-controlled chamber (HC), according to the ASTM D 2247 standard, was done.

3 Results and discussion

3.1 Characterization and electrochemical tests of the cleaned specimens

In Figure 1, the SEM micrographs of the cleaned specimens can be seen. After the polishing treatment, the P specimen surface shows streaks caused by the cleaning method. C and RCA specimens exhibited a topography formed by typical hexagonal platelets of zinc somewhat inclined with respect to the surface (Zhang 1996). Anodically clean (A) specimens show this structure, but the edges of the platelets are not so well defined, probable due to a significant quantity of oxides formed during the cleaning process. This cleaning anodic process dissolves the metal and forms oxides on the surface to enhance the number of OH groups that would increase the amount of possible coating-metal interactions (Zhang 1996).

Determined by EDS, the highest oxygen concentration, related to the number of oxides formed on the surface, was found in the A specimens due to the substrate oxidation during the cleaning treatment. Even though the RCA specimens showed the lowest oxygen concentration, its value was very close to that of the P and C specimens, Table 1.

The cathodic CV of the cleaned specimens showed significant differences (Figure 2). E_{op} values were more cathodic for P specimens (–1.03 V) and shift to more positive values and very similar for the C and A specimens (–0.79 V and –0.76 V, respectively), and even more positive for the RCA specimens (–0.69 V). The different values of E_{op}

Table 1: Oxygen concentration determined by EDS, estimated surface tension and contact angle of the specimens with the different surface treatments.

Specimen	Surface preparation	Oxygen At. (%)	Surface tension (dyn/cm)	Contact angle (°)
P	Polishing	5.6	31.2 – 33.7	81.05
C	Electrochemical cathodic cleaning	5.1	36 – 41.9	39.15
A	Electrochemical anodic cleaning	8.2	47.3 – 53.4	14.51
RCA	Oxidizing cleaning	4.8	47.3 – 53.4	23.41

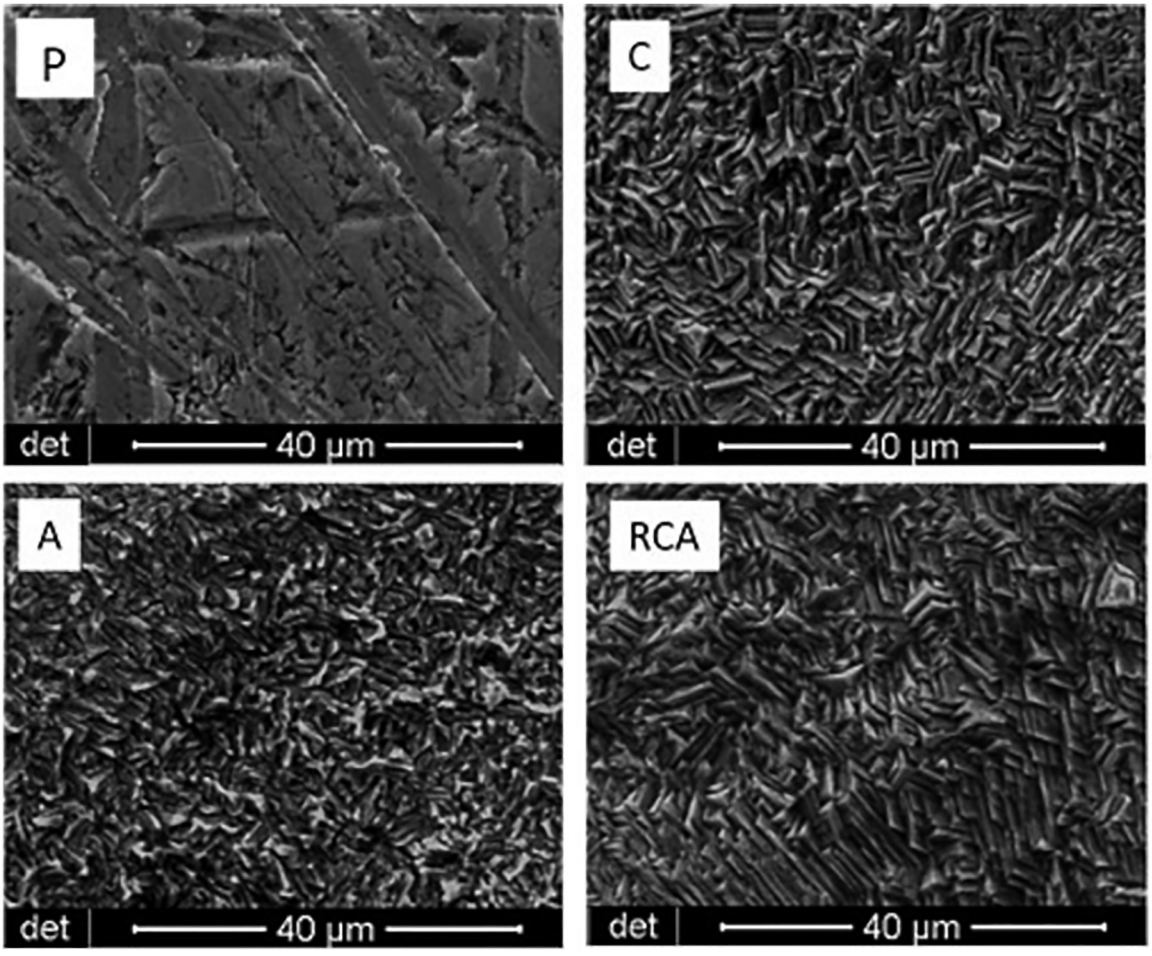

Figure 1: SEM photographs of specimens after the surface cleaning process and before the silane application.

indicates that the zinc oxides/hydroxides generated on the specimens' surface were different for each surface preparation. In addition, the specific charge values [Q ($C.cm^{-2}$)] for the cathodic peak (Cp), assigned to the reduction of previously formed oxides/hydroxides (Jiang et al. 2012), were different in each case.

These results show that either the oxides/hydroxides species type, their amount on the substrate, morphology or passivation mechanisms are different in each type of cleaning performed, due to the different reaction environment (Zhang 1996). According to the specific charge determination (area under the cathodic peak), the ranking of the oxides/hydroxides amount developed on each specimen surface was A > C > P > RCA, similar to that obtained with EDS oxygen analysis. On the other hand, considering the E_{op} of each specimen (the RCA E_{op} was the most anodic) and the Q values of the oxides/hydroxides´ dissolution (RCA had the lowest value of Q), it is concluded that the film formed with the RCA® cleaning is the thinnest and the most compact. The diluted RCA® solution concentration and the temperature of the chemical treatment mark the characteristics of the oxides/hydroxides film (Najari et al. 2009).

EIS is a technique very sensitive to the surface condition. Consequently, the results of the EIS measurements, after 20 min of immersion in diluted NaCl solution, showed significant differences (Figure 3). The impedance module evolution presented in the Nyquist diagrams was similar for the P, C and A specimens. At low frequencies, a not well-defined trending to the matter transfer as the limiting step of the corrosion rate can be seen; this is a typical behavior of zinc surfaces with a uniform oxides/hydroxides film (Zhang 1996).

Distinctly, the RCA specimens presented an inductive loop at low frequencies (Deslouis et al. 1989; Sziráki et al. 2001). This loop indicates that the increase of the oxidation current is impeded. Several studies have attributed this fact to the adsorption of Zn(I) and Zn(II) intermediaries during Zn dissolution (Cai and Park 1996; Deslouis et al. 1989; Sziráki et al. 2001). In this case, the dissolution may be limited by the diffusion process due to the adsorbed film.

Equivalent electrical circuits were chosen to represent the evaluated systems, considering the number of time constants observed in the EIS measurements presented in Figure 3 and the actual physical characteristics of each system. The solution resistance (Rs) was similar for all the specimens. The electrical equivalent circuits (van Ooij and Zhu 2001; Yu et al. 2020) are shown in Table 2 together with the values of each component.

For P and A specimens the electrical equivalent circuit is based on two contributions: at high frequencies, the resistance R1 and the capacitance CPE1, are associated to the precipitation of $Zn(OH)_2$; at low frequencies, the contribution to the impedance is associated to the charge transfer resistance (R2) in parallel with the electrochemical double layer capacitance (CPE2) (Simões and Fernandes 2010). In the case of P specimens, after 20 min in contact with the NaCl electrolyte, the $Zn(OH)_2$ will rapidly precipitate on the bare metal surface since the surface remains highly activated after the mechanical polishing. On the A specimens´ surface a thicker oxides/hydroxides film is formed during the anodic cleaning process. It will act as a barrier to the electrolyte flux during the specimen immersion in the NaCl solution. The latter agrees with the higher R1 and lower CPE1 values obtained in the equivalent circuit analysis (Table 2).

C specimens present an equivalent circuit with three contributions (Table 2). At high and medium frequencies, the contributions are associated to the characteristic precipitates

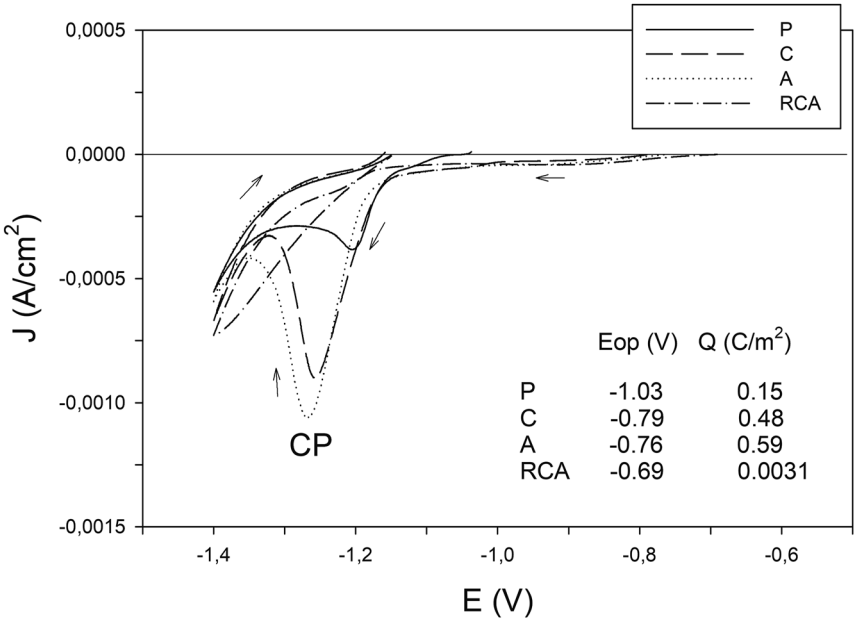

Figure 2: CV of the specimens after the surface cleaning process and before silane application.

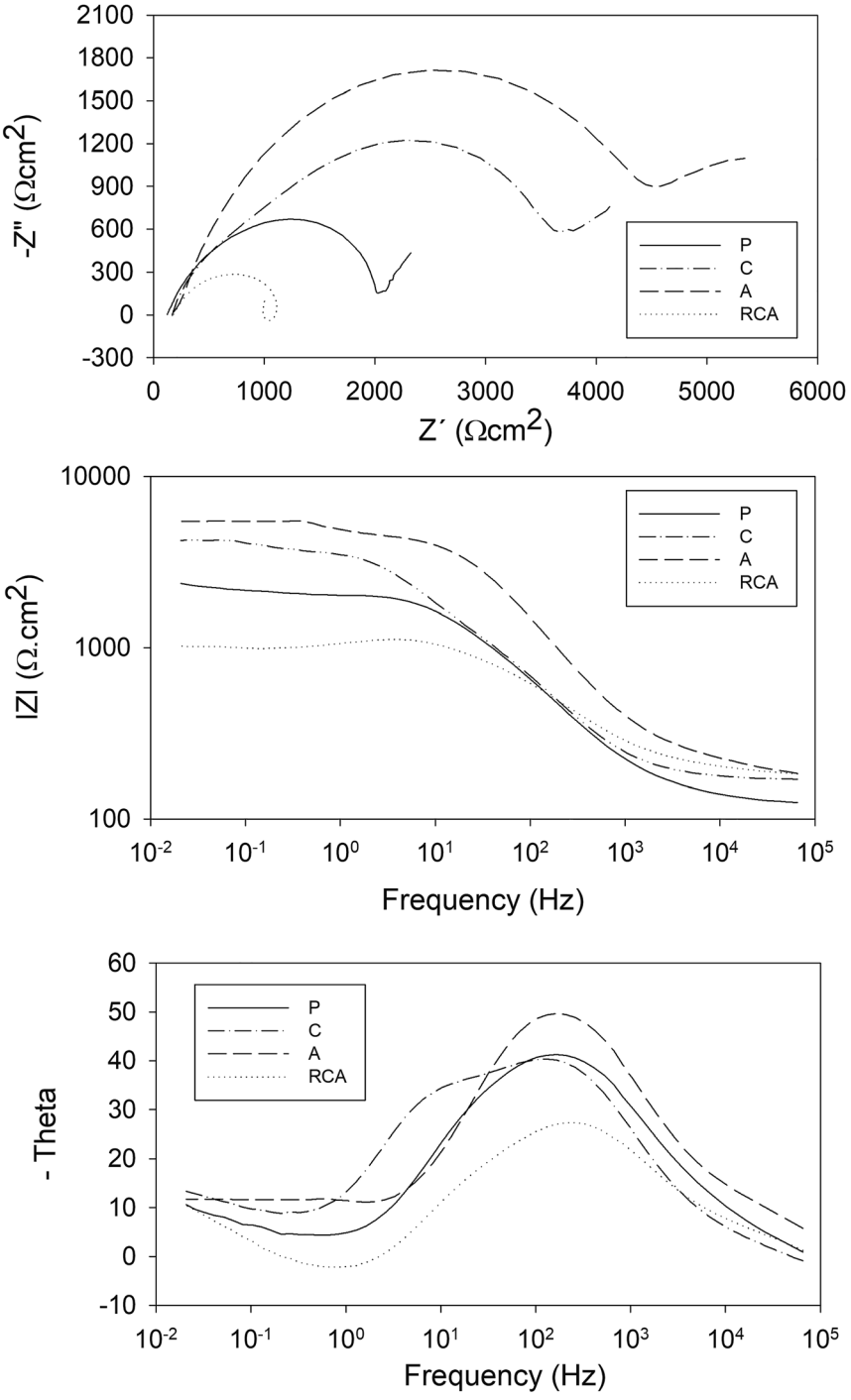

Figure 3: Nyquist and Bode diagrams of specimens with different surface cleaning after 20 min of immersion in NaCl solution.

formed on the surface (oxi/hydroxides films). Some authors claim that this could be related to a film consisting of two layers, being R1 and R2 their resistances (Kong et al. 2011). The time constant defined at high frequency represents the response of the coating outer layer, while that defined at the medium range would correspond to the inner layer, nearer to the substrate (Kong et al. 2011). Other authors indicate that this split is due to heterogeneities and the existence of different densities (dense or porous zones) in the film (Franquet et al. 2003; van Ooij and Zhu 2001). The low frequency contribution is associated to the faradaic process (charge transfer resistance, R3, and electrochemical double layer capacitance, CPE3).

The most probable equivalent circuit found for fitting the RCA specimens´ impedance data presents two contributions (Table 2). The high frequencies contribution is attributed to the barrier effect of the oxides/hydroxides film generated during the RCA® cleaning process (R1 and CPE1) and the second to the adsorption processes of reaction intermediaries generated during the zinc dissolution process and subsequently adsorbed on the electrode surface (L1 and

Table 2: Equivalent circuits and components values of the equivalent circuit of each system.

Specimen	*Rs* (Ω cm^2)	*R*1 (Ω cm^2)	CPE1 (Fcm^{-2})	*n*1	*R*2 (Ω cm^2)	*L*2 (H cm^{-2})	CPE2 (Fcm^{-2})	*n*2	*R*3 (Ω cm^2)	CPE3 (Fcm^{-2})	*n*3	Chi-squared
P	124.02	2039.97	1.57E-05	0.7	2221.23		1.07E-02	0.9				1.62E-03
C	168.54	1577.28	1.01E-05	0.77	3043.26		2.14E-03	0.83	2067	1.76E-05	0.87	3.16E-04
A	192.39	4611	4.72E-06	0.81	2385		2.52E-04	0.9				2.60E-04
RCA	179.67	825.21	2.39E-05	0.63	240.09	0.09						3.90E-03

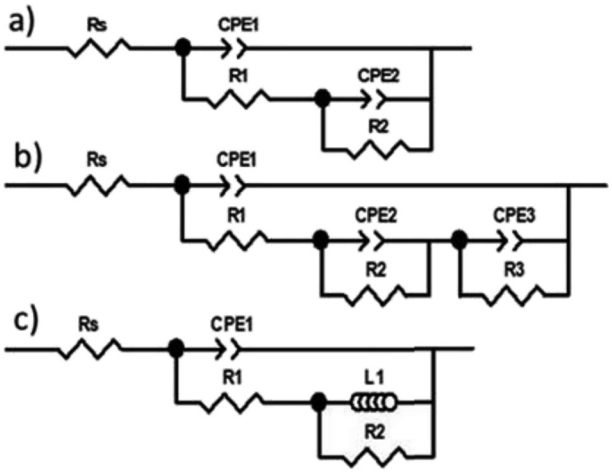

Specimen	Circuit
P	(a) Rs(CPE1[R1(R2CPE2)])
C	(b) Rs(CPE1[R1(R2CPE2) (R3CPE3)])
A	(a) Rs(CPE1[R1(R2CPE2)])
RCA	(c) Rs(CPE1[R1(R2L2)])

CPE2) (Cai and Park 1996; Salot et al. 1996). The R1 value is the lowest of the tested specimens, probably because the film formed during the cleaning process is very thin. This result agrees with the obtained in the CV test where this specimen showed the lowest specific charge (Q) (Figure 2).

Experimental data fitting with the equivalent electrical circuit models was performed and the experimental and fitted models were coherent. The obtained Chi-Squared values were included in Table 2.

The estimated surface energy and contact angles are shown in Table 1. Figure 4 shows the different contact angle of distilled water on the cleaned surfaces; important differences are observed. The surfaces better wetted by water correspond to the A or RCA as contact angles are near 20°, while the polishing treatment provided the lower wettability (higher contact angle).

Vuori et al. (2016) measured contact angle around 22°, after an alkaline cleaning process on galvanized steel. Nejad et al. (2022), employed different solutions of NaOH with and without acetylacetone and measured contacts angles among 82 and 65°. Both claimed that the low angles are due to hydroxylated surfaces. Vuori et al. (2016) also determined the resistance associated to the precipitation of $Zn(OH)_2$, R1, by EIS in 0.05 M NaCl (pH = 7) solution after 30 min. The value was 18 Ω cm^2, much lower than the ones obtained by the cleaning methods studied in this paper, indicating that the oxyhidroxyde film is more reactive (Vuori et al. 2016).

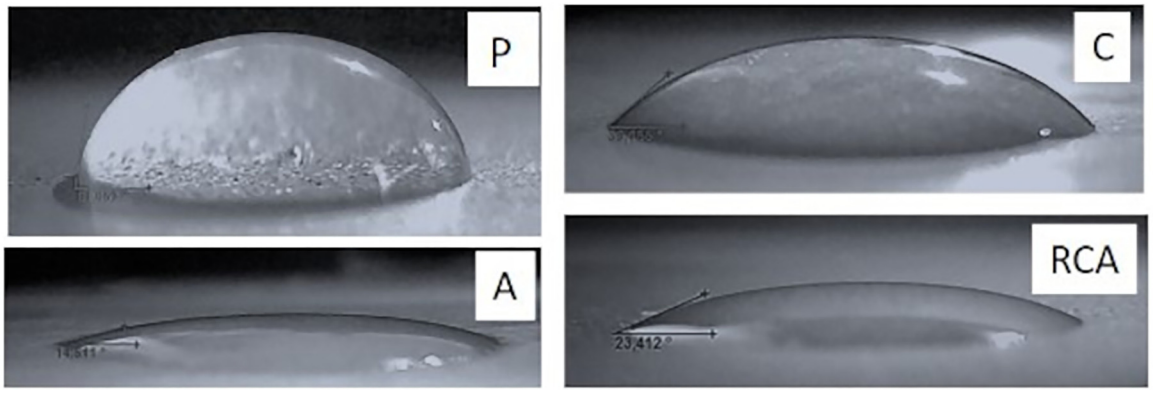

Figure 4: Photograph of a drop of distilled water applied to the specimens with different surface cleaning before the silane application.

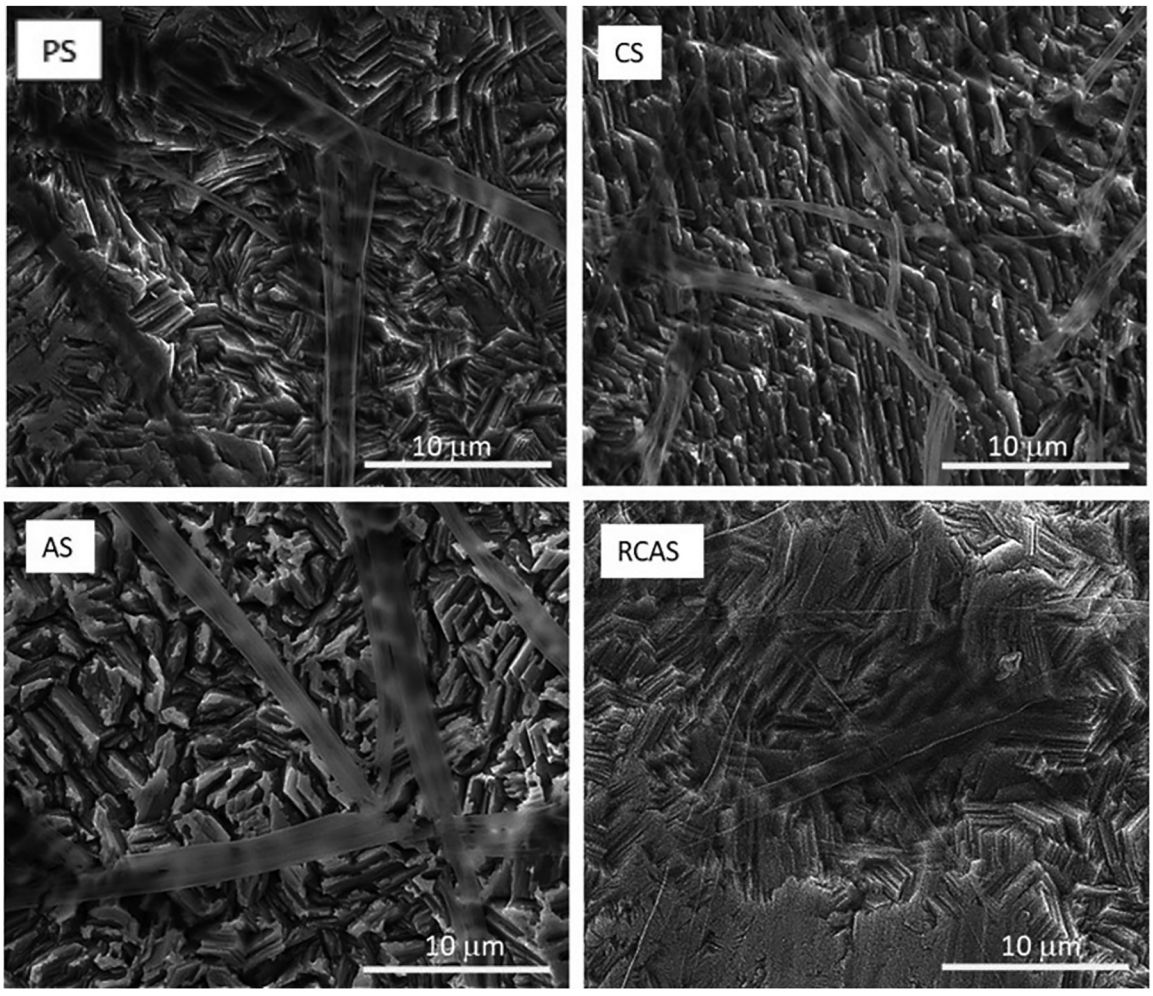

Figure 5: SEM micrograph of the specimens after the curing process of silane.

As the surface tension of the hydrolyzed APTES is 21.5 dyn/cm, hydrolyzed silane in all cases wet the surface ($\gamma_L <$ *ys*,), but the wetting is better in the case of the A and RCA specimens because these are more hydrophilic (greater difference between the surface tensions of the solid and the liquid).

These results showed that A and RCA specimens have similar hydrophilicity (probably due OH^- groups on the surface, according to the chemical reaction occurred during the cleaning processes). However, the cyclic voltammetry and EDS determinations showed that RCA had lower amount of oxides/hydroxides compounds, confirming that the protective film is the thinnest and the most compact one.

3.2 Characterization and electrochemical tests of specimens coated with APTES

Although silane-based coatings are very thin, the presence of a coating on the electrogalvanized surface was revealed in the SEM images of all the specimens (Figure 5). The characteristic substrate structure was less clearly observed in the coated specimens compared with the specimens without silane film (Figure 1). This indicates that the silane film was effectively formed. No cracks were detected.

In Table 3, chemical compositions determined by EDS can be seen. In all the cases the presence of Si is detected, confirming the formation of the silane film on the zinc surface. AS and RCAS comparatively showed higher Si content.

Table 3: Silicon and oxygen concentration determined by EDS after the silane curing and relative active surface of the tested coatings.

Specimen	Silicon At. (%)	Oxygen At. (%)	Relative active surface (%)
P	0.00	5.6	100
PS	2.34	6.73	6.8
CS	2.13	7.73	3.7
AS	2.85	7.13	0.9
RCAS	3.78	8.61	0.6
RCAS2L	6.96	7.29	0.3

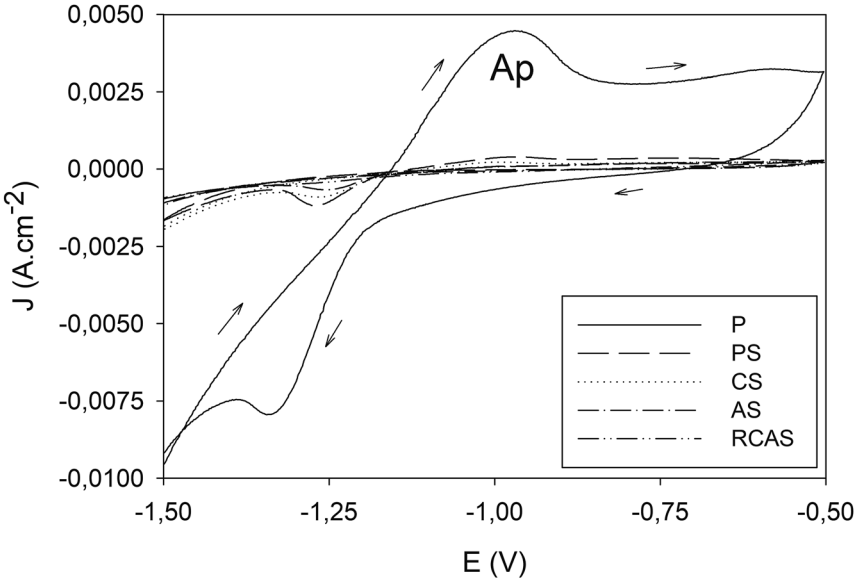

Figure 6: CV of the coated and uncoated electrogalvanized steel specimens.

This could indicate that the silane coatings formed after applying anodic or RCA® cleaning methods are thicker than those on the P and C specimens. This is in accordance with the better substrate wettability.

Regarding the substrate exposed area, Figure 6 displays that the CV of the control silane-free P specimens shows an anodic peak (Ap) at approximately –1.0 V/(SCE) followed by a passive region. This peak corresponds to the formation of a ZnO or $Zn(OH)_2$ film that blocks the electrochemically active surface, promoting the passivation process (Titz et al. 2010). The analysis of the curve with an anodic peak allows calculating the electrochemically active surface exposed to the electrolyte (Seré et al. 2014a). The specimens covered with silanes showed this Ap at the same potential but with lower activity than the P specimens.

It can be considered that P specimens have its whole geometric area electrochemically active, while silanes pretreated ones have partially blocked surfaces with reduced active area. The relative active surface exposed to the electrolyte (Ras) can be defined as:

$$\mathrm{Ras}_i = A^i \mathrm{Z_n} \big/ A^0 * 100 \tag{2}$$

where A^i_{Zn} is the zinc free active area on the (i) silane pretreated specimen, and A_0 is the specimen geometric area.

As the silane coating protects the substrate by barrier effect to the passage of ions from the electrolyte, the protection is related to the film coating surface. The evaluation of A^i_{Zn}, the zinc active area, for the different specimens could be performed from the CV curves. It is possible to evaluate the charge density [Q ($\mathrm{Ccm^{-2}}$)], related with the zinc anodic dissolution, from the area under the anodic peak (Ap). In the case of P specimens, it is possible to evaluate Q^0, associated to a completely free zinc surface, while for the other specimens the charge density will be Q^i, corresponding to the anodic charge associated to the zinc active area below the silane film.

By definition:

$$Q^i = q^i_{\mathrm{Zn}} \big/ A^0 \tag{3}$$

where q^i_{Zn} is the charge for the anodic process on the active free zinc surface of the (i) specimen and it can be shown as related to Q^0 through:

$$q^i_{Zn} = Q^0 * A^i_{\mathrm{Zn}} \tag{4}$$

Combining (3) and (4),

$$Q_i = Q^0 * A^i_{\mathrm{Zn}} \big/ A^0 \tag{5}$$

(Seré et al. 2014a) From Equation (2) and Equation (5) it is possible to obtain an electrochemical estimation of Ras as follows:

$$\mathrm{Ras}^i = Q^i \big/ Q^0 * 100 \tag{6}$$

The relative active surface exposed to the electrolyte was evaluated by calculating the ratio of the Ap area of each silane coated specimen and the Ap area of the P specimen (Table 3). As can be seen, the coated AS and RCAS specimens showed lower zinc active surface area than the other tested specimens. These results, added to the higher Si content detected by EDS in the AS and RCAS specimens, would indicate that the silane film formed on these specimens was thicker and more homogeneous than the one formed in the rest of the specimens.

The corrosion behavior of specimens coated with APTES was evaluated by exposure to the HC test. After 336 h of exposure, the coated RCAS specimens exhibit less signs of corrosion than the AS ones while those used as control

(P specimens) presented not only zinc corrosion products but also a significant amount of iron corrosion products on their surfaces. The PS specimens showed the worst protective behavior among all the specimens coated with silane, in agreement with the high exposed zinc surface (Figure 7). However, they showed a lower corrosion degree than the P specimens.

3.3 Characterization and electrochemical tests of specimens cleaned with RCA® and coated with two layers of APTES

In Section 3.2, the effect of different surface cleaning on the corrosion behavior of electrogalvanized steel coated with a layer of APTES was evaluated. It was found that the system with the best performance was the one cleaned with RCA®. For this reason, it was decided to apply two layers of APTES (RCAS2L) on RCA® cleaned specimens. They were characterized and their performance compared with RCAS.

Figure 8 shows a SEM image of the surface specimen with one and two layers of APTES. It can be observed that the typical structure of electrogalvanized steel appears more diffuse when APTES is applied in two layers (RCAS2L). This fact, added to that the Si content is considerably higher when a second silane layer is applied (Table 3), is indicative that the coating is thicker.

Furthermore, in the CV it is observed that both the current in the anodic swept and the area under the anodic peak are considerably lower in the RCAS2L specimens than in the RCAS ones (Figure 9), indicating that, when a second APTES layer is applied, the surface sites that had not been covered in

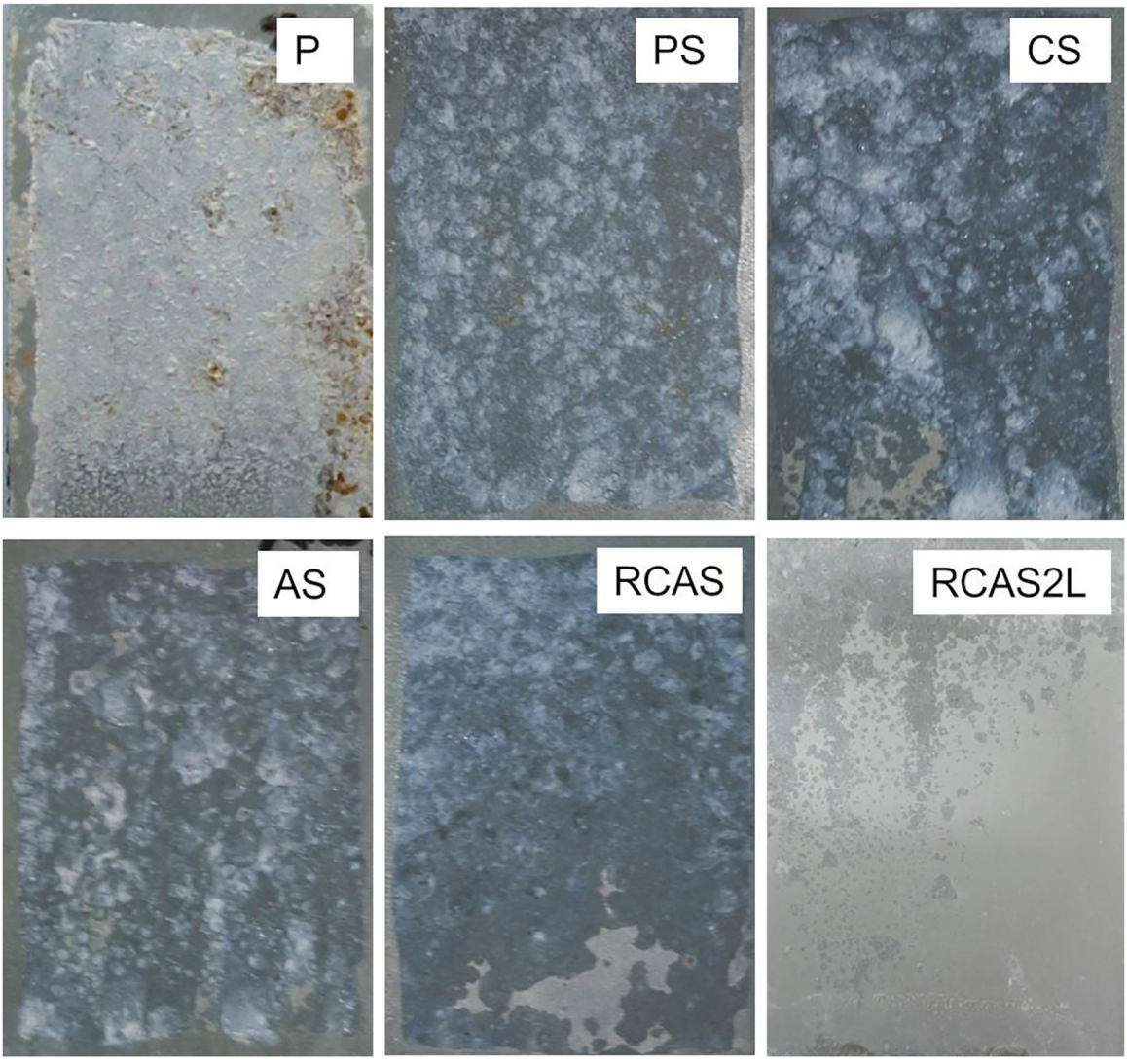

Figure 7: Photograph of the specimens exposed for 336 h in humidity chamber.

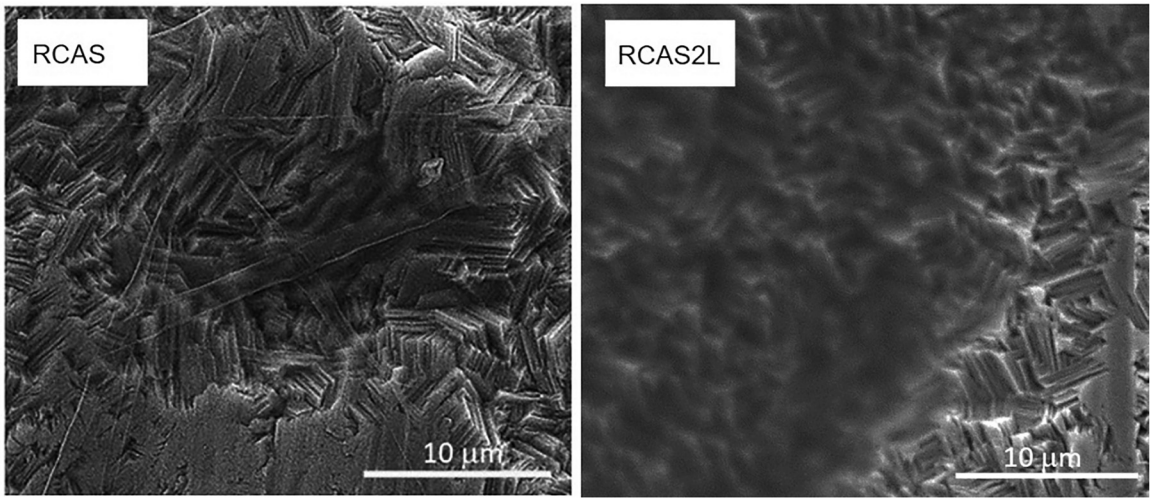

Figure 8: SEM micrograph of specimens cleaned with RCA® and coated with one or two layers of APTES.

the first silane solution immersion, are covered during the second one, lowering considerably the active area (Table 3).

Figure 10 shows the evolution of the Nyquist and Bode diagrams of the EIS determinations in the RCAS and RCAS2L specimens at different immersion times in NaCl. The values of the components corresponding to the equivalent circuits that represent the specimen's corrosion behavior are shown in Table 4. For RCAS2L, the best fit was obtained considering 2 times constants throughout the entire trial. This can be seen in the Bode diagram (Figure 10a). The system behavior is represented by the equivalent circuit of Table 4a). The same equivalent circuit represents the behaviour, in the early assay stages of RCAS specimens. The high-frequency constant (R1 y CPE1) represents the coating film resistive–capacitive characteristics. R1 symbolizes the coating resistance to the ionic flux, while the capacitance (CPE1) is associated to the electrolyte permeability in the film. Pores and/or other defects in the film generate paths through which the electrolyte can easily move toward the metallic substrate. As the electrolyte permeates through the coating, the tendency is an increase in the film capacitance (CPE1). Consequently, as the electrolyte permeates the coating through the pores and/or other defects, a drop in the R1 value occurs. Therefore, the evolution of this parameter is very important to evaluate the coating barrier performance in aqueous media. The resistive and capacitive components (R2 and CPE2) of the time constant at low frequencies represent the corrosion process development at the substrate/coating film interface. R2

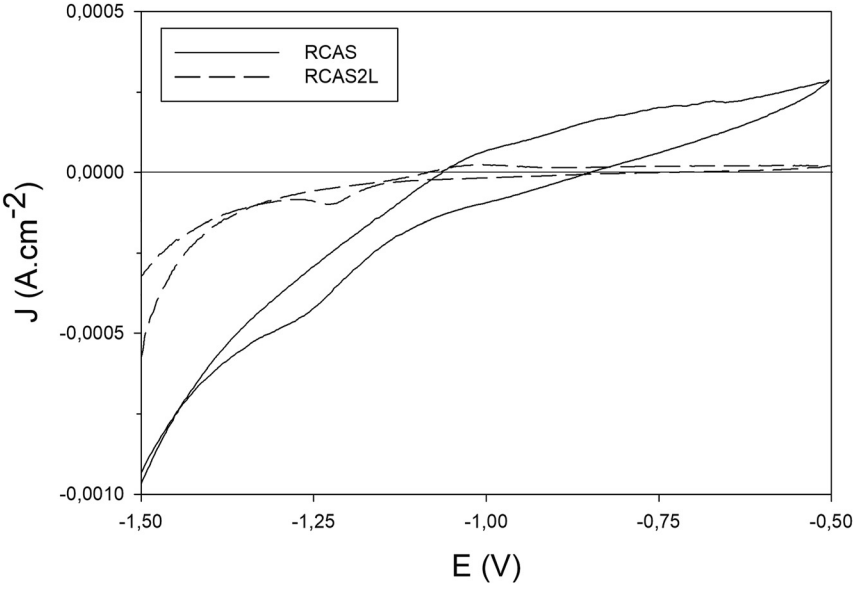

Figure 9: CV of specimens cleaned with RCA® and coated with one or two layers of APTES.

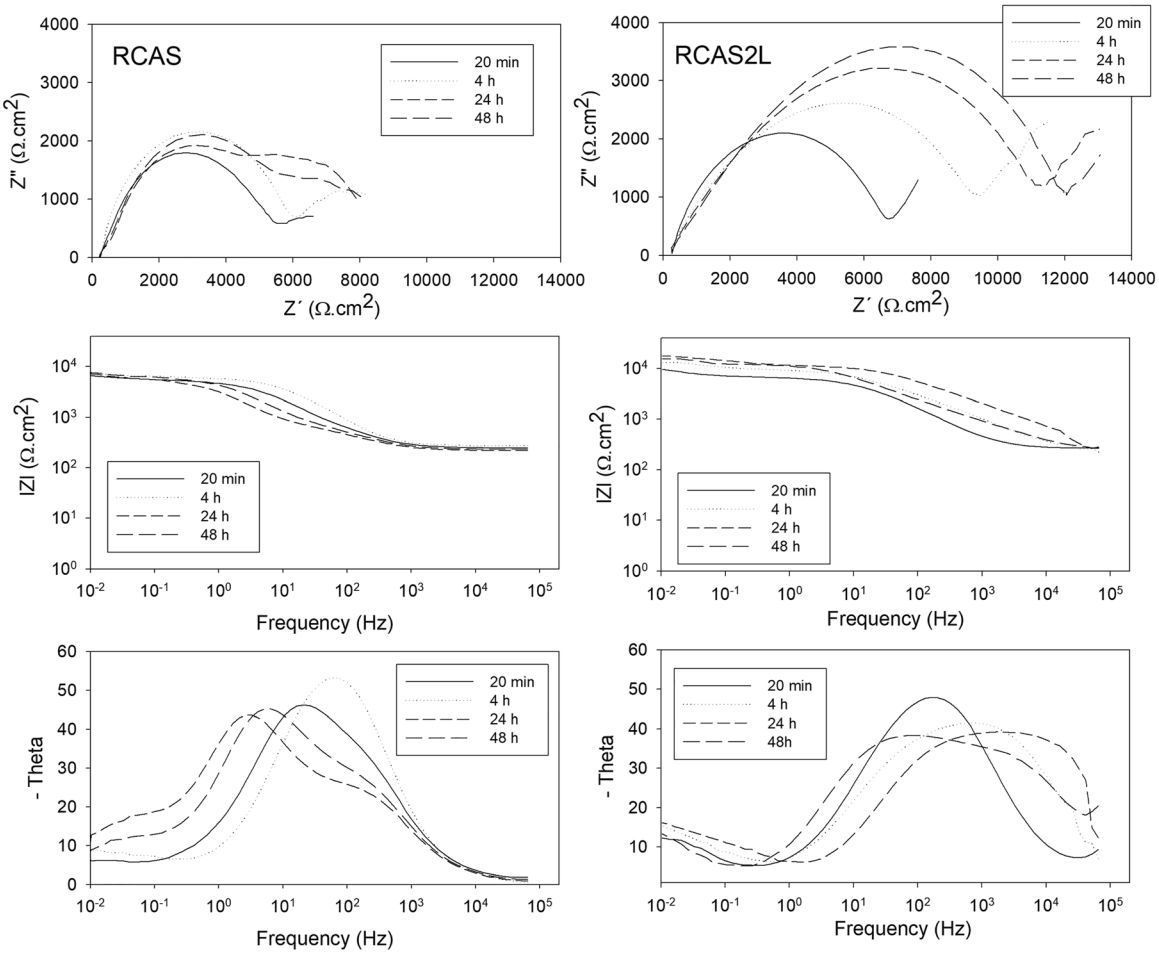

Figure 10: Nyquist and Bode diagrams of specimens cleaned with RCA® and coated with one or two layers of APTES at different times of immersion in NaCl solution.

Table 4: Components values of the equivalent circuit of one or two layers APTES.

RCAS time	*Rs* (Ω cm^2)	*R*1 (Ω cm^2)	CPE1 (Fcm^{-2})	*n*1	*R*2 (Ω cm^2)	CPE2 (Fcm^{-2})	*n*2	*R*3 (Ω cm^2)	CPE3 (Fcm^{-2})	*n*3	Chi-squared
20 min	243.0	5456.9	1.89E-05	0.72	1342.0	6.92E-03	0.96				0.0014
4 h	272.0	5571.4	5.66E-06	0.84	4030.7	6.29E-04	0.64				0.00023
24 h	216.6	645.5	1.89E-05	0.73	4696.9	3.71E-05	0.85	2871.5	3.14E-06	0.86	0.00086
48 h	229.4	853.8	1.70E-05	0.75	4867.0	1.57E-05	0.88	2621.9	1.19E-03	0.74	0.00015
RCAS time	***Rs*** **(Ω cm^2)**	***R*1 (Ω cm^2)**	**CPE1 (Fcm^{-2})**	***n*1**	***R*2 (Ω cm^2)**	**CPE2 (Fcm^{-2})**	***n*2**	***R*3 (Ω cm^2)**	**CPE3 (Fcm^{-2})**	***n*3**	**Chi-squared**
20 min	254.6	6485.6	5.03E-06	0.73	6409.3	1.45E-03	0.71				0.0016
4 h	205.6	9955.0	1.51E-05	0.6	4552.2	3.84E-03	0.96				0.00086
24 h	250.3	11,925.0	1.32E-05	0.62	4778.0	5.28E-03	0.95				0.0013
48 h	268.2	13,041.2	1.51E-05	0.62	4789.1	1.21E-02	0.99				0.0021

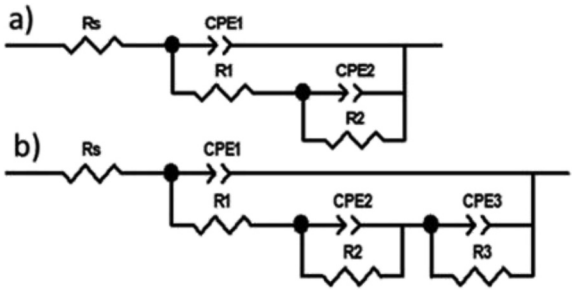

represents the charge transfer resistance and CPE2 the electrochemical double-layer capacitance.

At longer immersion times (24 and 48 h), the Bode diagram of RCAS specimens shows three-time constants (Figure 10b), which are represented in the equivalent circuit model shown in Table 4b). In the phase angle plot, peaks at high and medium frequencies are associated to the coating characteristics. As it was previously explained, some authors claim that such peaks could be related to heterogeneities and the existence of different crosslinking densities (dense or porous zones) inside the film (Franquet et al. 2003; van Ooij and Zhu 2001).

Vuori et al. (2016), informed that charge transfer resistance values, R1, of the specimens protected with a 3-aminopropyltrimethoxysilane film applied on an alkaline cleaned surface are 117–132 Ω cm^2 and 48 Ω cm^2, depending on the concentration of the silane in the hydrolyzed solution. They claimed that the main differences are due to the higher densely packed well-ordered monolayer of the first silane film while at higher silane concentration, a nanoporous film, which permits the diffusion of Cl^- ions is formed (Vuori et al. 2016).

Nejad et al. (2022), observed that the silane film (tetraethyl orthosilicate and 3-(chloropropyl)-trimethoxy silane), deposited on galvanized pretreated with 0.5 M NaOH (with or without acetyl acetone) solution has better uniformity and integrity of the silane film compared with other NaOH concentrations. EIS studies showed that this specimen a charge transfer resistances values around 1–5 kΩ cm^2, that, in general, increased as time elapsed (Nejad et al. 2022).

However, when 4 % v/v of silane solution was used, the charge resistance values were higher, between 5 and 0.8 kΩ cm^2 and diminished as time elapsed. This indicates that maybe in the case of the RAS cleaning method, an ordered silane film is obtained that gets disordered and porous at longer times.

During the assay, the electrolyte permeation through the film increases due to the increasing coating porosity and damage as it is hydrated. Furthermore, delamination at the coating/substrate interface can occurred, causing the electrochemically active area to increase as well (Zhang 1996). However, the corrosion products gathering on active sites could seal some pores. The total resistance (|Z| at low frequency) fluctuation is attributed to the antagonism of these processes. As seen in Figure 11, the |Z| values raised in the early assay stages in both specimens but more markedly in the RCAS2L. Then fell slightly in RCAS, indicating that the coating structure remains almost stable during the test. The electrolyte permeates through the film pores up to reach the substrate and creates the necessary and sufficient environmental conditions for the onset of corrosion. The corrosion products generated by this process seal the pores. The result is that |Z| value rises slightly again, stabilizing at 7759 Ωcm^2. In the case of RCAS2L, as the coating has a smaller active area, the effect of pores sealing is more relevant than in the case of RCAS. This fact is evidenced in |Z| steadily growth during the first 24 h of immersion and subsequent stabilization at 13,181 Ωcm^2 (Mrad et al. 2018; van Ooij and Zhu 2001).

After 336 h of exposure in the humidity and temperature-controlled chamber, the corrosion degree was lower in the RCAS2L specimens, only the upper part of the specimen showed precipitation of zinc corrosion products (white rust) (Figure 7). These results, added to those obtained by EIS, indicate that the presence of a second APTES layer considerably increases the system temporary corrosion resistance. This improvement is produced by increasing the silane film thickness (higher silicon content) and sealing the coating defects (lower active area) when a second layer is applied.

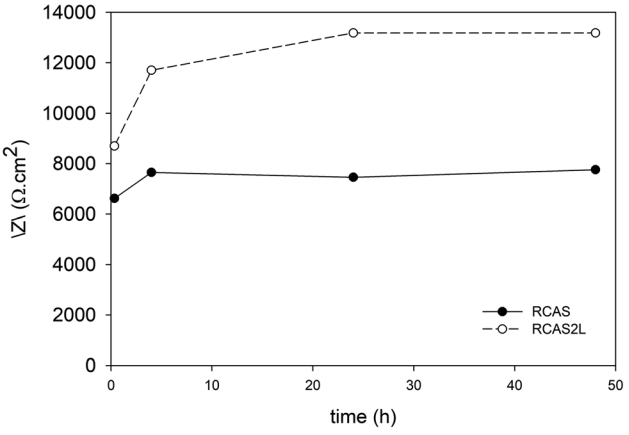

Figure 11: Evolution of low frequencies impedance modulus (|Z|) in the EIS assay.

3.4 Mechanism analysis

In the case of P and C specimens, a thin, porous oxides/hydroxides layer is formed, and the silane film deposited on them has no protective characteristics as important areas of bare metal are exposed: Ras = 6.8 and 3.7, respectively (Table 3). In the case of A specimens, the thicker oxides/hydroxides film, formed during the cleaning process, provided higher amount of OH^- ions to react with the silanols (8.2% of O on the metal surface), enhancing the Silica-Oxygen-Metal bonds. Due to the presence of OH^-, the film has good wettability: θ = 14.51° (Table 1). Consequently, a thicker and

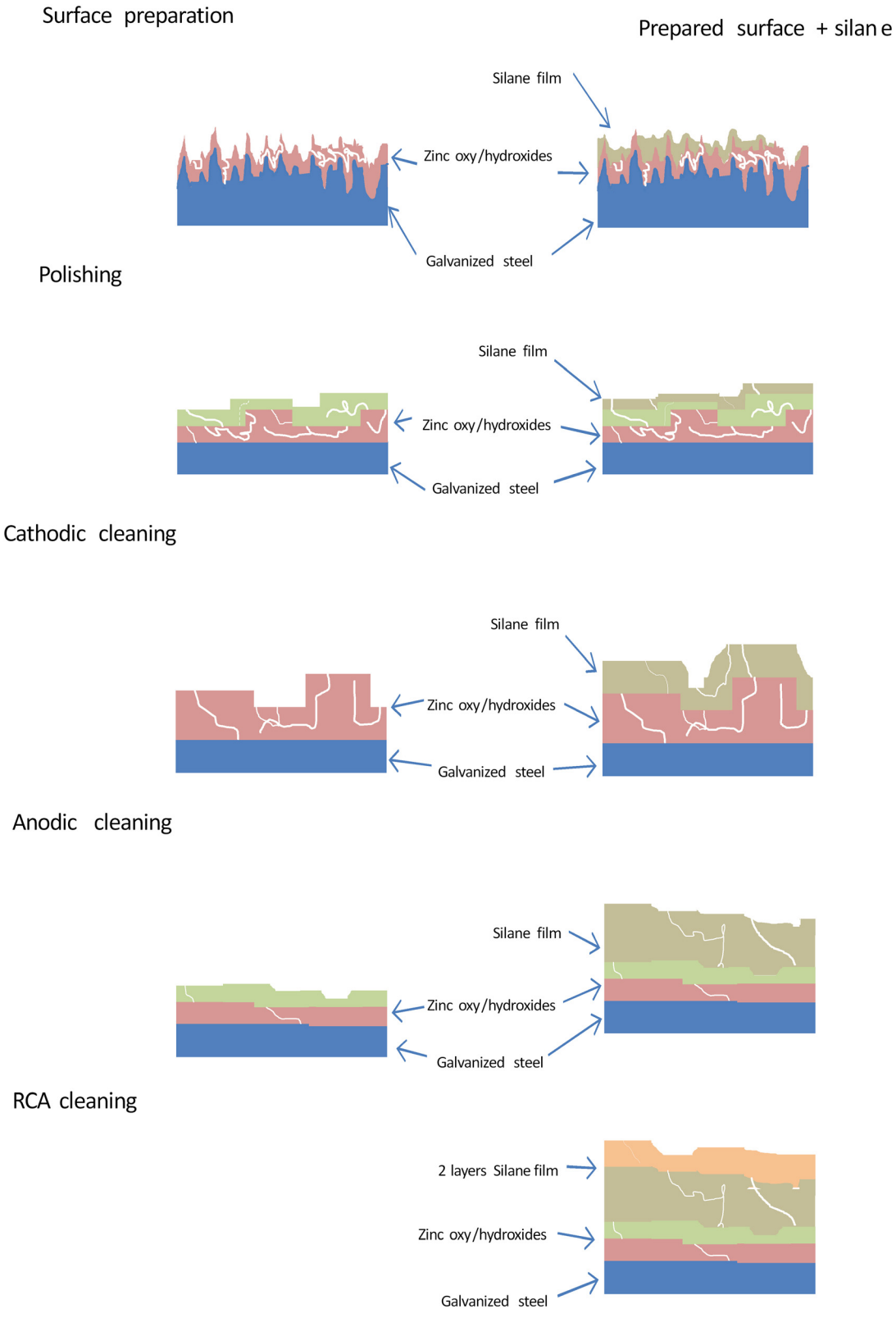

Figure 12: Scheme of the mechanism of protection of silane film.

more homogeneous silane film was deposited, giving better protection to the metal. On the other hand, the more compact and thinner oxides/hydroxides (4.8 % of O on the metal surface) film formed on RCA specimens, together with the thicker and more homogeneous silane film (Ras = 0.6), provided to the metal a good corrosion protection. In the case of RCAS2L, as the second silane film seals the porous and enhances the thickness of the first layer (6.96% of Si on the metal surface and Ras = 0.3), better protection is afforded.

A scheme of the mechanism is presented in protective Figure 12.

4 Conclusions

Several authors have used different zinc surface treatments before applying a silane film. In most of the experiments, different alkaline cleaning types were used while, in others, the galvanized specimens were kept at high temperature to form a film of oxides and, thus, activate the substrate surface. Through different methods, the aim of all the experiments was to generate an oxidized surface or to increase the presence of hydroxyl groups. The species (oxides/hydroxides) type, its morphology and amount available on the surface certainly significantly affects the characteristics of the deposited and cured silane film. This fact is evidenced in this work since specimens with different surface preparation showed different surface energy and reactivity due to the development of different oxides/hydroxides species on the zinc surface.

(1) All the surface cleaning methods provided a surface energy greater than the surface tension of the hydrolyzed APTES solution.
(2) All the APTES films formed on electrogalvanized steel sheets subjected to different types of surface cleaning provide a temporary protection effect against corrosion.
(3) No cracks were seen in the silane coatings.
(4) The surface treatment affects not only the coating silicon content but also the zinc exposed area.
(5) The most hydrophilic surfaces were those cleaned by RCA® or employing anodic current.
(6) Specimens cleaned by RCA® showed the greater surface energy and reactivity, allowing to obtain coatings with higher Si content, lower exposed zinc surface area and better performance against corrosion in an environment with high humidity.
(7) Double layer coating of APTES considerably increases the temporary resistance of electrogalvanized steel protection, due to the improvement of the coating barrier effect produced by the second APTES layer, which seals defects of the first one and increases its thickness.

Acknowledgements: The authors thank Andres Campbel from Camsi-X for providing the silane. Besides, the authors thank to the Comisión de Investigaciones Científicas de la Provincia de Buenos Aires (CICPBA), the Consejo Nacional de Investigaciones Científicas y Técnicas (CONICET), and the Universidad de La Plata (UNLP) for the financial support of this research.

Author contributions: All the authors have accepted responsibility for the entire content of this submitted manuscript and approved submission.

Research funding: This work was financially supported by CIDEPINT, the Comisión de Investigaciones Científicas de la Provincia de Buenos Aires (CICPBA), the Consejo Nacional de Investigaciones Científicas y Técnicas (CONICET), and the Universidad de La Plata (UNLP).

Conflict of interest statement: The authors declare no conflicts of interest regarding this article.

References

Akhtar, S., Matin, A., Madhan Kumar, A., Ibrahim, A., and Laoui, T. (2018). Enhancement of anticorrosion property of 304 stainless steel using silane coatings. Appl. Surf. Sci. 440: 1286–1297.

Alibakhshi, E., Akbarian, M., Ramezanzadeh, M., Ramezanzadeh, B., and Mahdavian, M. (2018). Evaluation of the corrosion protection performance of mild steel coated with hybrid sol-gel silane coating in 3.5 wt.% NaCl solution. Prog. Org. Coat. 123: 190–200.

Asadi, N. and Naderi, R. (2020). Nanoparticles incorporated in silane sol–gel coatings. In: Rajendran, S., Nguyen, T.A., Kakooei, S., Yeganeh, M., and Li, Y. (Eds.), *Corrosion protection at the nanoscale*. Elsevier, Netherlands.

Barceló, G., Sarret, M., Müller, C., and Pregonas, J. (1998). Corrosion resistance and mechanical properties of zinc electrocoatings. Electrochim. Acta 43: 13–20.

Cai, M. and Park, S.M. (1996). Oxidation of zinc in alkaline solutions studied by electrochemical impedance spectroscopy. J. Electrochem. Soc. 143: 3895–3902.

Calabrese, L. and Proverbio, E. (2019). A brief overview on the anticorrosion performances of sol-gel zeolite coatings. Coatings 9: 409.

Chico, B., de la Fuente, D., Pérez, M.L., and Morcillo, M. (2012). Corrosion resistance of steel treated with different silane/paint systems. J. Coat. Technol. Res. 9: 3–13.

Dave, B.C., Hu, X.K., Devaraj, Y., and Dhali, S.K. (2004). Sol–gel-derived corrosion-protection coatings. J. Sol-Gel Sci. Technol. 32: 143–147.

Deslouis, C., Duprat, M., and Tournillon, C. (1989). The kinetics of zinc dissolution in aerated sodium sulphate solutions. A measurement of the corrosion rate by impedance techniques. Corros. Sci. 29: 13–30.

Einati, H., Mottel, A., Inberg, A., and Shacham-Diamand, Y. (2009). Electrochemical studies of self-assembled monolayers using impedance spectroscopy. Electrochim. Acta 54: 6063–6069.

Figueira, R.B. (2020). Hybrid sol-gel coatings for corrosion mitigation: a critical review. Polymers 12: 689.

Franquet, A., Le Pen, C., Terryn, H., and Vereecken, J. (2003). Effect of bath concentration and curing time on the structure of non-functional thin organosilane layers on aluminium. Electrochim. Acta 48: 1245–1255.

Freund, B.B. and Freund, H.Z. (1930). A theory of the ring method for the determination of surface tension. J. Am. Chem. Soc. 52: 1772–1782.

GaoZhang, Z.D., Liu, Z., Li, X., Jiang, S., and Zhang, Q. (2019). Formation mechanisms of environmentally acceptable chemical conversion coatings for zinc: a review. J. Coat. Technol. Res. 16: 1–13.

Gladkikh, N., Makarychev, Y., Petrunin, M., Maleeva, M., Maksaeva, L., and Marshakov, A. (2020). Synergistic effect of silanes and azole for enhanced corrosion protection of carbon steel by polymeric coatings. Prog. Org. Coat. 138: 105386.

Hesamedini, S. and Bund, A. (2019). Trivalent chromium conversion coatings. J. Coat. Technol. Res. 16: 623–641.

Jeyaram, R., Elango, A., Siva, T., Ayeshamariam, A., and Kaviyarasu, K. (2020). Corrosion protection of silane based coatings on mild steel in an aggressive chloride ion environment. Surf. Interfaces 18: 100423.

Jiang, L., Wolpers, M., Volovitch, P., and Ogle, K. (2012). An atomic emission spectroelectrochemical study of passive film formation and dissolution on galvanized steel treated with silicate conversion coatings. Surf. Coat. Technol. 206: 3151–3157.

Jussila, P., Ali-Löytty, H., Lahtonen, K., Hirsimäki, M., and Valden, M. (2010). Effect of surface hydroxyl concentration on the bonding and morphology of aminopropylsilane thin films on austenitic stainless steel. Surf. Interfaces Anal. 42: 157–164.

Kern, W. (1990). The evolution of silicon wafer cleaning technology. J. Electrochem. Soc. 137: 1887–1892.

Khramov, A.N., Voevodin, N.N., Balbyshev, V.N., and Mantz, R.A. (2005). Sol–gel-derived corrosion-protective coatings with controllable release of incorporated organic corrosion inhibitors. Thin Solid Films 483: 191–196.

Kong, G., Liu, L., Lu, J., Che, C., and Zhong, Z. (2011). Corrosion behavior of lanthanum-based conversion coating modified with citric acid on hot dip galvanized steel in aerated 1M NaCl solution. Corros. Sci. 53: 1621–1626.

Krzak, J., Szczurek, A., Babiarczuk, B., Gąsiorek, J. and Borak, B. (2020). Sol–gel surface functionalization regardless of form and type of substrate. In: Hussain, C.M. (Ed.). *Handbook of nanomaterials for manufacturing applications*. Elsevier, The Netherlands.

Magalhães, A.A.O., Margarit, I.C.P., and Mattos, O.R. (1999). Electrochemical characterization of chromate coatings on galvanized steel. Electrochim. Acta 44: 4281–4287.

Mrad, M., Ben Amor, Y., Dhouibi, L., and Montemor, M.F. (2018). Effect of AA2024-T3 surface pretreatment on the physicochemical properties and the anticorrosion performance of poly(γ-glycidoxypropyltrimethoxysilane) sol-gel coating. Surf. Interface Anal. 50: 335–345.

Najari, A., Lang, P., Lacaze, P.C., and Mauer, D. (2009). A new organofunctional methoxysilane bilayer system for promoting adhesion of epoxidized rubber to zinc. Prog. Org. Coat. 64: 392–404.

Najari, A., Lang, P., Lacaze, P.C., and Mauer, D. (2012). Adsorption of 3-mercaptopropyltrimethoxysilane on zinc: a study of the competition between thiol and silanol functions related to the age of the siloxane solution, its pH and the oxidation state of the surface. Surf. Sci. 606: 137–145.

Nejad, S.A.T., Alibakhshi, E., Ramezanzadeh, B., Marhamati, F., Olivier, M.-G., and Mahdavian, M. (2022). The role of acetylacetone in alkaline surface modification bath of electro-galvanized steel to enhance protective functioning of a hybrid silane coating. Prog. Org. Coat. 171: 107048.

Niknahad, M. and Mannari, V. (2016). Corrosion protection of aluminum alloy substrate with nano-silica reinforced organic–inorganic hybrid coatings. J. Coat. Technol. Res. 13: 1035–1046.

Nikpour, S., Naderi, R., and Mahdavian, M. (2018). Fabrication of silane coating with improved protection performance using Mentha longifolia extract. J. Taiwan Inst. Chem. Eng. 88: 261–276.

Owczarek, E. (2019). Methods of modifying anticorrosive protective properties of silane films. Acta Phys. Pol. 135: 147–152.

Pathaka, S.S., Khanna, A.S., and Sinhab, T.J.M. (2006). Sol gel derived organic-inorganic hybrid coatints. A new era in corrosion protection of material. Corros. Rev. 24: 281–306.

Peng, T. and Man, R. (2009). Rare earth and silane as chromate replacers for corrosion protection on galvanized steel. J. Rare Earths 27: 159–163.

Prane, J.W. (1986). *Introduction to polymers and resins*. Springer, Switzerland.

Public Health Service (U.S.) (2010). *Toxicological profile for chromium*. Agency for Toxic Substances. Rule No. ASTSDR/TP-88/10, Atlanta, Georgia, USA.

Ramezanzadeh, B., Akbarian, M., Ramezanzadeh, M., Mahdavian, M., Alibakhshi, E., and Kardar, P. (2017). Corrosion protection of steel with zinc phosphate conversion coating and post-treatment by hybrid organic-inorganic sol-gel based silane film. J. Electrochem. Soc. 164: C224–C230.

Salot, R., Lefebvre-Joud, F., and Baroux, B. (1996). Electrochemical behavior of thin anodic oxide films on zircaloy. 4. Role of the mobile defects. J. Electrochem. Soc. 143: 3902–3909.

Saravanan, P. and Srikanth, S. (2019). Post treatment of hot dip galvanized steel sheet-chromating, phosphating and other alternative passivation technologies. J. Mater. Sci. Appl. 3: 101–123.

Seré, P.R., Deyá, C., Egli, W.A., Elsner, C.I., and Di Sarli, A.R. (2014a). Protection of galvanized steel with silanes: its comparison with chromium(VI). J. Mater. Eng. Perf. 23: 342–348.

Seré, P.R., Deyá, C., Elsner, C.I., and Di Sarli, A.R. (2014b). Behavior of two eco-compatible duplex systems used in the construction industry against corrosion. Int. J. Adhes. Adhes. 50: 1–6.

Seré, P.R., Banera, M., Egli, W.A., Elsner, C.I., Di Sarli, A.R., and Deyá, C. (2016). Effect on temporary protection and adhesion promoter of silane nanofilms applied on electro-galvanized steel. Int. J. Adhes. Adhes. 65: 88–95.

Simões, A.M. and Fernandes, J.C.S. (2010). Studying phosphate corrosion inhibition at the cut edge of coil coated galvanized steel using the SVET and EIS. Prog. Org. Coat. 69: 219–224.

Sundararajan, G.P. and van Ooij, W.J. (2000). Silane based pretreatments for automotive steels. Surf. Eng. 16: 315–320.

Sziráki, L., Szocs, E., Pilbáth, Z., Papp, K., and Kálmán, E. (2001). Study of the initial stage of white rust formation on zinc single crystal by EIS, STM/AFM and SEM/EDS techniques. Electrochim. Acta 46: 3743–3754.

Thai, T.T., Trinh, A.T., and Olivier, M.G. (2020). Hybrid sol–gel coatings doped with cerium nanocontainers for active corrosion protection of AA2024. Prog. Org. Coat. 138: 105428.

Tiringer, U., van Dam, J.P.B., Abrahami, S.T., Terryn, H., Kovač, J., Milošev, I., and Mol, J.M.C. (2021). Scrutinizing the importance of surface chemistry versus surface roughness for aluminium/sol-gel film adhesion. Surf. Interfaces 26: 101417.

Titz, T., Hörzenberger, F., Van den Bergh, K., and Grundmeier, G. (2010). Correlation of interfacial electrode potential and corrosion resistance of plasma polymer coated galvanized steel. Part 2: influence of forming induced defects. Corros. Sci. 52: 378–386.

van Dam, J.P.B., Abrahami, S.T., Yilmaz, A., Gonzalez-Garcia, Y., Terryn, H., and Mol, J.M.C. (2020). Effect of surface roughness and chemistry on the adhesion and durability of a steel-epoxy adhesive interface. Int. J. Adhes. Adhes. 96: 102450.

van Ooij, W.J. and Zhu, D. (2001). Electrochemical impedance spectroscopy of bis-[triethoxysilypropyl]tetrasulfide on Al 2024-T3 substrates. Corrosion 57: 413–427.

van OoijZhu, W.J.D.Q., Prasad, G., Jayaseelan, S., Fu, Y., and Teredesai, N. (2000). Silane based chromate replacements for corrosion control, paint adhesion and rubber bonding. Surf. Eng. 16: 386–396.

van Ooij, W.J., Zhu, D., Stacy, M., Seth, A., Mugada, T., Gandhi, J., and Puomi, P. (2005). Corrosion protection properties of organofunctional silanes: an overview. Tsinghua Sci. Technol. 10: 639–664.

Vuori, L., Ali-Löytty, H., Lahtonen, K., Hannula, M., Lehtonen, E., Niu, Y., and Valden, M. (2016). Improved corrosion properties of hot dip galvanized steel by nanomolecular silane layers as hybrid interface between zinc and top coatings. Corrosion 73: 169–180.

Wang, D. and Bierwagen, G.P. (2009). Sol–gel coatings on metals for corrosion protection. Prog. Org. Coat. 64: 327–338.

Wang, L., Liu, C.S., Yu H.Y., and An, C.Q. (2012). Structure and corrosion resistance of a composite γ-amino propyl triethoxy silane and γ-glycidoxy propyl trimethoxy silane conversion coating on galvanized steel. J. Iron Steel Res. Int. 19: 46–51.

Wang, X.X., Cao, Y.Q., Fu, H.L., Jiang, M.Y., and Hu, J.M. (2019). Understanding the role of silane pretreatments in an organic coating system. Part 1: corrosion performance and interfacial property. J. Coat. Technol. Res. 16: 881–893.

Younis, A.A., Ensinger, W., El-Sabbah, M.M.B., and Holze, R. (2013). Corrosion protection of pure aluminium and aluminium alloy (AA7075) in salt solution with silane-based sol–gel coatings. Mater. Corros. 64: 276–283.

Yu, Z., Hu, J., and Meng, H. (2020). A review of recent developments in coating systems for hot-dip galvanized steel. Front. Mater. 7: 74.

Zandi Zand, R., Flexer, V., De Keersmaecker, M., Verbeken, K., and Adriaens, A. (2016). Self-healing silane coatings of cerium salt activated nanoparticles. Mater. Corros. 67: 693–701.

Zeller, R.L. and Savinell, R.F. (1986). Interpretation of A.C. impedance response of chromated electrogalvanized steel. Corros. Sci. 26: 389–399.

Zhang, X.G. (1996). *Corrosion and electrochemistry of zinc*. Springer, New York, USA.

Zhao, Y., Cao, Y.Q., Wang, X.X., Chen, Y.Q., Liu, Y.C., and Hu, J.M. (2021a). Beneficial effect of pre-oxidization process on the formation of silane films on iron. Surf. Coat. Technol. 412: 127057.

Zhao, Z., Tabish, M., Zhao, J., Anjum, M.J., Wang, W., Wei, S., and Asl, V.Z. (2021b). Preparation and characterization of Nd-doped double-layer silane anticorrosion coating on AZ91D magnesium alloy surface. Corros. Rev. 39: 361–371.